S100A4 Silencing Facilitates Corneal Wound Healing After Alkali Burns by Promoting Autophagy via Blocking the PI3K/Akt/mTOR Signaling Pathway

Yulin Wang,[1] Guiping Gao,[1] Ying Wu,[2] Yuqin Wang,[3] Xiaorong Wu,[1] and Qiong Zhou[1]

[1]Department of Ophthalmology, First Affiliated Hospital of Nanchang University, Nanchang, P.R. China
[2]Department of Otolaryngology, First Affiliated Hospital of Nanchang University, Nanchang, P.R. China
[3]State Key Laboratory of Ophthalmology, Optometry and Visual Science, Eye Hospital of Wenzhou Medical University, Wenzhou, P.R. China

Correspondence: Yulin Wang, Department of Ophthalmology, First Affiliated Hospital of Nanchang University, No. 17, Yongwaizheng Street, Nanchang, 330006, P.R. China; drwangyulin19@163.com.

Received: November 8, 2019
Accepted: June 21, 2020
Published: September 14, 2020

Citation: Wang Y, Gao G, Wu Y, Wang Y, Wu X, Zhou Q. S100A4 silencing facilitates corneal wound healing after alkali burns by promoting autophagy via blocking the PI3K/Akt/mTOR signaling pathway. *Invest Ophthalmol Vis Sci.* 2020;61(11):19. https://doi.org/10.1167/iovs.61.11.19

Purpose. This study investigated the role of S100 calcium binding protein A4 (S100A4) in corneal wound healing and the underlying mechanism of the S100A4-mediated PI3K/Akt/mammalian target of rapamycin (mTOR) pathway.

Methods. The rabbit corneal alkali burn model was established in vivo. S100A4 expression, wound healing, inflammation, and autophagy in rabbit cornea after alkali burn were detected. The NaOH-treated rabbit corneal stromal cells (rCSCs) were transfected with overexpressed S100A4 or silencing S100A4 to examine the effect of S100A4 on corneal wound healing in vitro. The effect of S100A4 on cell viability, proliferation, migration, invasion, fibrosis, and autophagy of rCSCs after alkali burn was analyzed. Then the functional rescue experiments were carried out. The PI3K inhibitor, LY294002, was used to elucidate the PI3K/Akt/mTOR signaling pathway in rCSCs.

Results. S100A4 silencing promoted rabbit corneal wound healing by inhibiting fibrosis and inflammation and promoting autophagy in alkali-burned cornea, corresponding to increased levels of LC3, Beclin 1, and Atg4B but lowered α-smooth muscle actin, TNF-α, and p62 levels. Moreover, silencing S100A4 inhibited proliferation, migration, invasion, and fibrosis of NaOH-treated rCSCs and promoted the differentiation of rCSCs into corneal cells and the autophagy of damaged rCSCs. The inhibitory role of S100A4 in wound healing was achieved via activation of the PI3K/Akt/mTOR pathway.

Conclusions. S100A4 silencing confers a promising effect on wound healing of alkali-burned cornea by blocking the PI3K/Akt/mTOR pathway, supporting the advancement of corneal gene therapies for wound healing.

Keywords: alkali burns, corneal wound healing, S100A4, PI3K/Akt/mTOR signaling pathway, autophagy, corneal stromal cells

Alkali burn to the cornea is one of the most devastating chemical ocular burns, which damages the corneal epithelium and penetrates into the cornea.[1] Corneal wound healing is associated with complex mechanisms that cover cell death, migration, proliferation, and differentiation.[2] Dexamethasone and doxycycline have a protective effect on preservation of corneal clarity and improvement of wound healing after alkali burn.[3] Despite of significant advancement, the therapeutic agents used to improve corneal healing have not lived up to expectations thus far.[4] Recently, researchers have evaluated the efficacy of corneal gene therapy for corneal diseases or injuries in vitro and in vivo.[5]

S100 proteins, a family of calcium-binding proteins, implicate in a variety of cellular behaviors such as signaling, growth, differentiation, and motility.[6] S100A proteins participate in inflammation-related corneal neovascularization (CNV). For instance, S100A8 or S100A9 is viewed as a target for the treatment of diseases involving CNV.[7] Elevation of S100A8 and S100A9 is observed in some inflammatory ocular diseases, including xerophthalmia, meibomian gland dysfunction, and CNV.[8] As a major member of the S100 family, S100A4 protein is localized in the keratocyte phenotypes that emerge in corneal stromal tissues recovering from injury.[9] S100A4 is also a potent protein that triggers inflammation and production of cytokines and growth factors under various pathologic conditions.[10] Strikingly, our previous study has demonstrated that S100A4 silencing functions as a suppressor in CNV following alkali burn in vivo.[11] S100A4 is also introduced as a therapeutic target for neurodegeneration diseases, which may be a vital mediator for central nervous system injury.[12] Activation of Akt proteins may be a significant therapeutic approach for corneal wound healing, along with the healing of other tissues such as the skin.[13] An activated PI3K/Akt signaling pathway caused by phosphatase and tensin homologue deleted on chromosome 10 may be associated with enhanced cell migration and wound healing.[14] Activation of the the PI3K/Akt/mammalian target of rapamycin (mTOR)

signaling pathway is engaged in S100A4-mediated migration of colorectal cancer cells,[15] which may raise a potential mechanism involving the corneal repair following alkali burn. In view of this, our study aimed to examine the effect of S100A4 on corneal alkali burn in a rabbit model and a corneal stromal cell (rCSC) model, with the aim to explore the potential therapies for alkali-burned corneas.

Materials and Methods

Ethics Statement

This study was approved and supervised by the Ethics Committee of the First Affiliated Hospital of Nanchang University (Nanchang, China). All the animal experiments were conducted in accordance with the ARVO Statement for the Use of Animals in Ophthalmic and Vision Research. Significant efforts were made to minimize the number of animals and their sufferings.

Vector Construction

Total RNA was extracted and reverse transcribed to cDNA. The reaction system consisted of 2 µL 5 × Primer Script Buffer, 0.5 µL Primer Script RT Enzyme Mix, 0.5 µL Random 6 mers, 0.5 µL OligodT Primer, 1 µL total RNA, and 5.5 µL dH_2O. Reaction conditions were set as at 37°C for 30 minutes and at 85°C for 5 minutes. PCR amplification was performed. A forward primer sequence containing a *Nco*I restriction endonuclease cleavage site (5'-AGTCCCATGGCGTGCCCTCTGGAG-3') and a reverse primer sequence containing a *Xho*I restriction endonuclease cleavage site (5'-CGACCTCGAGTCATTTCTTCCTGGGCTGCTT-3') were synthesized and designed. The 25-µL PCR system included 12.5 µL Taq Master Mix, 1.0 µL PCR forward primer, 1.0 µL PCR reverse primer, 2.0 µL cDNA, and 8.5 µL dH_2O. Reaction conditions were set as predenaturation at 95°C for 3 minutes, 35 cycles of denaturation at 95°C for 30 seconds, annealing at 60°C for 30 seconds and extension at 72°C for 45 seconds, and a final extension at 72°C for 5 minutes. The PCR product was purified using a gel extraction kit, and the purified product was detached with *Nco*I and *Xho*I. The detached DNA fragments were ligated into pET28a$^+$ vector using T4 ligase. The vector expressing *S100A4* was transformed into *Escherichia coli* DH5α, and the constructed pET28a-S100A4 vector was amplified and verified by sequencing.

According to the S100A4 gene sequence in GeneBank, the short hairpin RNA (shRNA) sequence targeting S100A4, GTGACAAGTTCAAGCTCAA, was designed according to the shRNA design principle, and the GeneBank verified that there was no homology with the gene sequence other than *S100A4*. A primer sequence encoding *S100A4* shRNA was synthesized based on the RNA interference sequence. Sense-*S100A4* (5'-GATCCGTGACAAGTTCAAGCTCAATTCAAGAGATTGAGCT-TGAACTTGTCACTTTTT-3') and antisense-*S100A4* (5'-AGCTTAAAAAAGTGACAAGTTCAAGCTCAATCTCTTGAAT-TGAGCTTGACG-3') were resuspended to 10 µmol/L using 10 mmol/L Tris-HCl (pH 8.0). The forward and reverse primers were mixed at 1:1 and heated to 95°C for 3 minutes. The annealed double-stranded DNA was ligated with the product recovered from PLKO.1 vector by AgeI and EcoRI double-enzyme digestion under the action of T4 ligase. The ligated product was transformed into the receptive cell Stbl3. The monoclonal colonies were selected for amplification and identified by bacterial liquid PCR. *S100A4* shRNA vector was extracted for sequencing verification.

Rabbit Corneal Alkali Burn Model

A total of 65 healthy New Zealand white rabbits (34 females and 31 males, aged 80–90 days, weight 1.8–2.5 kg) were purchased from Shanghai Slack Laboratory Animal Co., Ltd. (Shanghai, China). The rabbits were anesthetized with 20 mg/kg ketamine. The eyeballs of rabbits were normal and healthy without corneal damage or scar under a slit-lamp microscope. Among the 65 white rabbits, 15 were randomly selected as the controls, and the remaining 45 were used for the alkali burn model establishment. The filter paper (5 mm in diameter) was immersed in 2 mol/L NaOH solution and then put on the eyeballs of the white rabbits for 40 seconds. Thereafter, the filter paper was removed and residual NaOH solution was washed away with normal saline. Subsequently, the rabbits with corneal alkali burn were randomly divided into the alkali treatment (AT) group, empty vector (EV) group, and shRNA-*S100A4* group (sh group for short), with 15 rabbits in each group. The cornea of each rabbit in the sh group was injected with 10 µL *S100A4* shRNA. Eight quadrant bulbar conjunctiva of each rabbit in the EV group were injected with 10 µL empty plasmid. Each rabbit in the AT group was injected with 10 µL normal saline. On days 1, 3, 7, 14, and 28 after the Schirmer test, the corneas were excised from three white rabbits: corneas from one eye of the three rabbits were used for frozen sections, and corneas from the other eye of the three rabbits were used for extraction and quantification of protein and RNA, as well as extraction of the aqueous humor for ELISA.

Schirmer Test

One end of a 5 × 35-mm sterile filter paper was folded at a right angle at 5 mm. The folded end of the filter paper was placed on the inside one-third lower jaw. The long end was suspended outside the eyelid, and the length of the wet filter paper (excluding the 5-mm folded end) was recorded after 5 minutes.

ELISA

The content of TNF-α in aqueous humor was measured using a double-antibody sandwich ELISA kit (Shanghai Bogoo Biotechnology Co., Ltd., Shanghai, China).

Quantitative RT-PCR

Total RNA was extracted from cells and corneas using a TRIzol kit (TAKARA, Otsu, Shiga, Japan). Subsequently, formaldehyde gel electrophoresis was used to verify the reliability of the obtained RNA. Reverse transcription was then performed using the PrimeScript RT kit (TAKARA) in strict accordance with the instructions. mRNA expression was quantified by standard real-time quantitative PCR (qPCR) methods using SYBR Premix Ex Taq (TAKARA). β-Actin was used as a reference gene. Primers are shown in Table 1.

Western Blot Assay

Total protein was extracted by radio-immunoprecipitation assay lysis buffer containing phenylmethanesulfonyl

Investigative Ophthalmology & Visual Science

Table 1. Primer Sequences for RT-qPCR

Primer	Sequence
S100A4	F: GGGCAAAGAGGGTGACAAGTTC
	R: CTGGGCTGCTTATCTGGGAAG
VEGF	F: CTTGCTGCTCTACCTCCACC
	CTTTGGTCTGCATTCACATTTG
TNF-α	F: ATGAGCACGGAAAGCATGATCC
	R: AGGGCAAGGCTCTTGATGGCAG
Vimentin	F: GGACCAGCTAACCAACGACA
	R: AAGGTCAAGACGTGCCAGAG
Col I	F: GGGATTCCCTGGACCTAAAG
	R: GGAACACCTCGCTCTCCA
Col III	F: CTGGACCCCAGGGTCTTC
	R: CATCTGATCCAGGGTTTCCA
α-SMA	F: CTGAGGACTATGGGGTCATC
	R: TAGTGCCCATCATTCTTGGT
CD34	F: TCTTGACAACAACGGTACTGCTAC
	R: GCTGGTACTTCCAAGGGTACTAGG
KERA	F: GAAGGCAAGGTGGTATAATGG
	R: ACAATCAAAGTCATCCGCAC
LUM	F: CCATCGATGCCACCATGGAGACAGAC
	R: ACGCGTCGACCAGATCCTCTTCTGAGATG
COL5A1	F: AAGCGTGGGAAACTGCTCTCCTAT
	R: AGCAGTTGTAGGTGACGTTCTGGT
ALDH1A1	F: CAAAGACCTCGATAAAGCCGT
	R: ACCATATTCTCCCAGTTCTCGT
ALDH3A1	F: CGAGTACGTGGTGGAATC
	R: AGGGATGATGTTCTGGGC
LC3	F: AAGGCGCTTACAGCTCAATG
	R: CTGGGAGGCATAGACCATGT
BECLIN	F: AGGTTGAGAAAGGCGAGACA
	R: AATTGTGAGGACACCCAAGC
p62	F: TGAGGAACAGATGGAGTCGG
	R: GAGATGTGGGTACAAGGCAG
ATG4B	F: TCCATAGGCCAGTGGTACG
	R: TGCACAACCTTCTGATTTCC
β-actin	F: ACAGTCAGCCGCATCTTCTT
	R: GACAAGCTTCCCGTTCTCAG

ALDH1A1, aldehyde dehydrogenase 1 family member A1; *ALDH3A1*, aldehyde dehydrogenase 3 family member A1; *ATG4B*, autophagy-related 4B cysteine peptidase; *BECLIN*, autophagy-related 6; *Col I*, type I collagen; *Col III*, type III collagen; *COL5A1*, collagen type V alpha 1 chain; *KERA*, keratocan; *LUM*, lumican; *LC3*, light chain 3; *S100A4*, S100 calcium binding protein A4.

fluoride (Beyotime, Beijing, China). The protein concentration was determined by standard bicinchoninic acid assay. An equal amount of protein (50 µg) was subjected to 10% SDS-PAGE and then transferred to polyvinylidene fluoride (PVDF) membranes (Millipore, Billerica, MA, USA) after electrophoresis. The PVDF membranes were incubated with Tris-buffered saline Tween-20 (Boster, Wuhan, China) containing 5% skim milk at room temperature to block nonspecific binding. Membranes were then incubated with primary antibodies (Table 2) overnight at 4°C and incubated with rabbit anti-mouse secondary antibody for 1 hour at room temperature. Protein bands were visualized by enhanced chemiluminescence and imaged using a BioSpectrum gel imaging system (Bio-Rad, Hercules, CA, USA).

Hematoxylin and Eosin Staining

The frozen cornea sections were prepared, immersed in hematoxylin staining solution for 5 minutes, and washed with running water to remove floating color. Then sections were differentiated in 1% hydrochloric acid alcohol for a few seconds, washed in running water for 15 minutes, dyed with eosin for 2 minutes, color separated with 95% alcohol for 1 minute, dehydrated with gradient alcohol, cleared with xylene, and observed under a microscope after sealing with neutral gum.

Table 2. Antibodies for Western Blot Assay

Antibody	No. Company	Dilution Ratio
VEGF	ab32152, Abcam	1:5000
S100A4	ab124805, Abcam	1:1000
TNF-α	ab66579, Abcam	1:100
α-SMA	ab32575, Abcam	1:5000
Col I	ab34710, Abcam	1:5000
Col III	ab184993, Abcam	1:5000
CD34	ab81289, Abcam	1:10,000
Kera	ab8068, Abcam	1:5000
Lum	ab188348, Abcam	1:5000
Col5A1	ab112551, Abcam	1:100
ALDH1A1	ab227948, Abcam	1:10,000
ALDH3A1	ab76976, Abcam	1:1000
LC3	ab48394, Abcam	1:2000
Beclin	ab207612, Abcam	1:2000
Atg4B	ab154843, Abcam	1:10,000
p62	ab91526, Abcam	1:100
PI3K	ab76234, Abcam	1:1000
p-PI3K	ab182651, Abcam	1:1000
AKT	ab8805, Abcam	1:500
p-AKT	ab38449, Abcam	1:1000
mTOR	ab2732, Abcam	1:2000
p-mTOR	ab109268, Abcam	1:10,000
β-actin	ab179467, Abcam	1:5000

rCSC Culture and Transfection

The eyeballs were removed as soon as the rabbits were killed by air embolism, and the corneal epithelium and endothelium were scraped off with a sterile surgical blade. The remaining corneal stromal tissues were cut into 2 × 2-mm pieces and washed with PBS two to three times. The tissue blocks were dissolved with 1.5g/L type I collagenase solution and centrifuged at 1000 r/min for 5 minutes. Then, the supernatant was discarded. The diluted rCSCs were cultured in Dulbecco's modified Eagle's medium (DMEM)/F12K medium supplemented with 10% FBS at 37°C with 5% CO_2. When the cells reached a confluence of 85%, the cells were passaged at 1:3. The cells of P3 generation were treated with 0.5 mol/L NaOH to establish an alkali-burn model in rCSCs. Afterward, alkali-burn rCSCs were transfected with the constructed S100A4 shRNA vector, S100A4 overexpression vector, or empty vector, which were recorded as the sh group, OE group, and NC group respectively. The rCSCs after alkali burn added with PBS were set as a blank control and recorded as the rCSC group. Quantitative RT-PCR (RT-qPCR) and Western blot experiments were performed according to the methods described above.

5-Ethynyl-2′-Deoxyuridine Labeling Assay

Cell proliferation was detected by the 5-ethynyl-2′-deoxyuridine (EdU) assay as previously described.[16]

Immunocytochemistry

Cell slides were incubated in 3% hydrogen peroxide deionized water for 5 to 10 minutes at room temperature to eliminate endogenous peroxidase activity. After being rinsed

Table 3. Antibodies for Immunofluorescence Assay

Antibody	No. Company	Dilution Ratio
E-cadherin	ab1416, Abcam	1:100
Vimentin	ab119139, Abcam	1:100
Ki67	ab32575, Abcam	1:5000
FSF-3	ab184993, Abcam	1:5000
FSP-1	ab1416, Abcam	1:50
LC3B	ab18203, Abcam	1:100

FSF-3, fruitless stimulation factor 3; LC3B, light chain 3B.

with PBS, the slides were incubated with biotin-labeled goat anti-rabbit primary antibody against vimentin at 37°C for 15 minutes. After PBS washes, the slides were incubated with horseradish-labeled streptavidin working solution at 37°C for 15 minutes. Following PBS washing again, the slides were developed with diaminobenzidine. After being rinsed with running water, the slides were counterstained with hematoxylin for 5 minutes and turned to blue under the treatment of distilled water for 15 minutes. Subsequently, the slides were dehydrated in gradient alcohol, cleared with xylene, and sealed with neutral gum, followed by observation under a microscope.

Immunofluorescence

The rinsed cells on the glass cover slides were fixed with 4% paraformaldehyde at 4°C for 15 minutes and treated with 0.5% Triton X-100 for 20 minutes. The primary antibodies against vimentin, FSF-3, FSP-1, and LC3 (Table 3) were added for incubation overnight at 4°C. The cells were washed with PBS and incubated with fluorescent goat anti-mouse secondary antibody for 1 hour at 37°C. The cells were observed under a fluorescence microscope.

3-(4,5-Dimethylthiazol-2-yl)-2,5-Diphenyltetrazolium Bromide Assay

Cells in logarithmic phase were detached with trypsin and dispersed into a single-cell suspension of 1×10^4 cells/mL using DMEM/F12K medium containing 10% FBS. The cells were seeded into a 96-well plate, 200 µL (2×10^3 cells) per well. The cell-free culture medium was added to blank wells as the blank control. Five parallel wells were set in each group, and the cells were cultured in an incubator containing 5% CO_2 at 37°C for 0 to 7 days. After 0, 24, 48, and 72 hours of culture, 20 µL of 5 mg/mL 3-(4,5-dimethylthiazol-2-yl)-2,5-diphenyltetrazolium bromide (MTT) solution was added to each well for another 4 hours of incubation, followed by the discarding of supernatant. Then, each well was added with 200 µL dimethyl sulfoxide and shaken for 10 minutes to fully dissolve the crystals. The optical density of each well was measured at a wavelength of 490 nm.

Flow Cytometry

The cells in good condition were washed with PBS, detached with 0.025% trypsin, and then cultured with DMEM/F12K containing 2 mmoL carboxyfluorescein diacetate succinimidyl ester (CFSE) (Invitrogen, Carlsbad, CA, USA) for 15 to 30 minutes. The cells were washed three times with PBS. The supernatant was discarded after centrifugation. The solution was resuspended in DMEM/F12K. The CFSE-labeled cells were detected on the flow cytometer.

Calcein-Acetoxymethylester Staining

Cells were rinsed twice with PBS and stained with 2 µmol calcein-acetoxymethylester (calcein-AM) staining solution (Biovision, Mountain View, CA, USA) for 15 minutes. Then the staining solution was washed away with PBS, and the cells were observed under a fluorescence microscope.

Scratch Test

The six-well plate was seeded with 5×10^5 cells per well and incubated at 37°C with 5% CO_2 for 24 hours. Subsequently, a scratch was made on the single layer of cells using a 1-mL pipette, and images were captured under a microscope at 0, 12, and 24 hours to calculate the relative cell migration distance.

Transwell Assay

Each apical Transwell chamber was coated with Matrigel (BD Biosciences, Franklin Lakes, NJ, USA) for 30 minutes of incubation under aseptic conditions, added with 30 µL RPMI-1640 medium, and then placed in a CO_2 incubator. The cells were detached, centrifuged, resuspended with serum-free medium, and diluted into cell suspension at 5×10^5 cells/mL. Next, 500 µL RPMI-1640 medium containing 10% FBS was added to each basolateral chamber, and a 200-µL cell suspension was added to each apical chamber, followed by incubation at 37°C for 48 hours with 5% CO_2. Afterward, the medium was washed away with PBS and the cells were stained with crystal violet for 10 minutes. The crystal violet on the surface was washed away with running water, and the cells in the apical chamber were wiped off with a cotton swab. Cells that invaded through the Matrigel were counted with images captured under a microscope.

Transmission Electron Microscopy

Cells were fixed with glutaraldehyde dissolved in ethidium bromide (a final concentration of 1.25%) at 25°C for 1 hour and embedded in epoxy resin. The embedded cells were sectioned and stained with uranyl acetate and lead citrate. The stained cells were visualized on a JEOL 1200EX transmission electron microscope (Jeol Ltd. Tokyo, Japan).

Statistical Analysis

Data were analyzed using SPSS 21.0 statistical software (SPSS, Inc., Chicago, IL, USA). The data showed a normal distribution by Kolmogorov-Smirnov test. Measurement data were expressed as mean ± standard deviation. Comparisons between two groups were analyzed using the *t*-test. The comparisons among multiple groups were analyzed by one-way or two-way ANOVA with Tukey's multiple comparisons test used for pairwise comparison. Enumeration data were compared using Fisher's exact test. A two-sided *P* value <0.05 indicated a statistically significant difference.

Investigative Ophthalmology & Visual Science

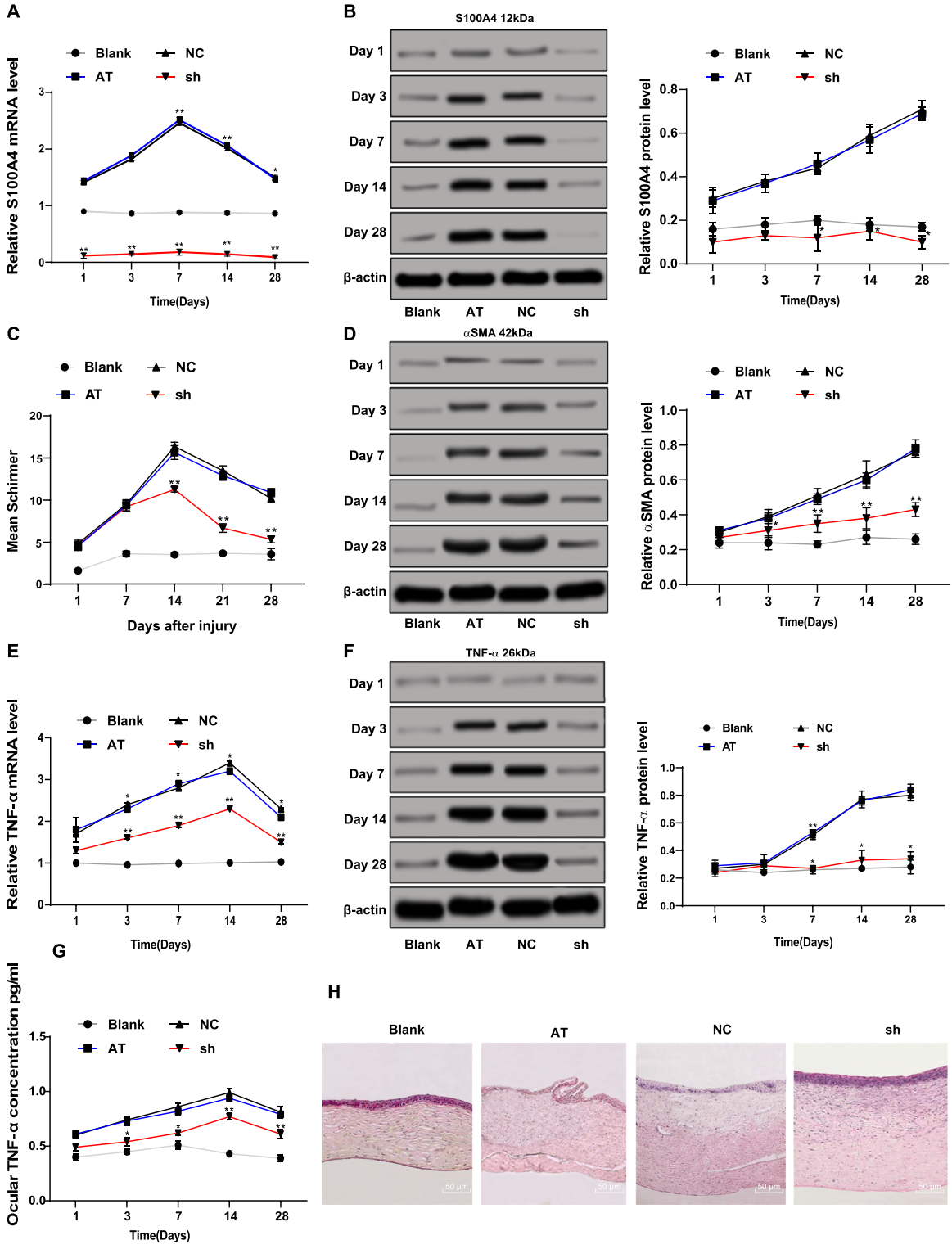

Figure 1. Silencing S100A4 contributed to promotion of corneal wound healing after alkali burn. The mRNA (**A**) and protein (**B**) levels of *S100A4* (S100A4) in rabbit cornea measured by RT-qPCR and Western blot assay; formation of tears detected using the Schirmer test (C); the protein level of α-SMA in rabbit cornea measured by Western blot assay (**D**); the mRNA (**E**) and protein (**F**) levels of *TNF*-α (TNF-α) in rabbit cornea measured by RT-qPCR and Western blot assay; the protein concentration of TNF-α in aqueous humor measured by ELISA assay (**G**); hematoxylin and eosin staining was carried out on the cornea to observe the inflammatory cells in cornea at day 28 (**H**). $n = 3$. On days 1, 3, 7, 14, and 28, three New Zealand white rabbits from each group were used for the Schirmer test, and corneal tissue was extracted for RT-qPCR and Western blot assay. Data are expressed as mean ± standard deviation. Two-way ANOVA and Tukey's multiple comparisons test were used for data analysis. $^{*}P < 0.05$. $^{**}P < 0.01$.

Investigative Ophthalmology & Visual Science

Table 4. Assessment for Corneal Clarity of Rabbits After Alkali Burn

Group	Days	Class 0: Iris Details Clearly Visible	Class I: Opacity Causes Blurriness of Iris Details	Class II: Pupil Discernible Despite Opacity	Class III: Unable to Discern Pupil; Complete Opacity	*P*
Blank		15/15				
AT			3/15	12/15		
NC	1		4/15	11/15		<0.05
si			13/15	2/15		
Blank		15/15				
AT			2/15	10/15	3/15	
NC	3		1/15	10/15	4/15	<0.01
si			6/15	8/15	1/15	
Blank		15/15				
AT				5/15	10/15	
NC	7			4/15	11/15	<0.01
si			6/15	9/15		
Blank		15/15				
AT				2/15	13/15	
NC	14			3/15	12/15	<0.01
si			6/15	7/15	2/15	
Blank		15/15				
AT			4/15	11/15		
NC	28		5/15	10/15		<0.01
si		12/15	3/15			

NC, negative control; si, small interfering RNA targeting S100A4.

Results

S100A4 Silencing Improves Corneal Wound Healing Against Alkali Burn

The mRNA and protein levels of *S100A4* (S100A4) in the cornea after alkali burn were determined by RT-qPCR and Western blot assay. The results showed that *S100A4* (S100A4) levels in the AT group were higher than those in the blank group at days 1, 3, 7, 14, and 28, whereas *S100A4* (S100A4) levels were reduced at each time point in the sh group compared with those in the NC group (Figs. 1A, 1B). The wound healing of the rabbit cornea after alkali burn was observed. It was found that the corneal wound healing of rabbits with alkali burn in the sh group after 3 days was better than that in the NC group (Table 4). Considering that corneal damage can lead to an abnormal increase

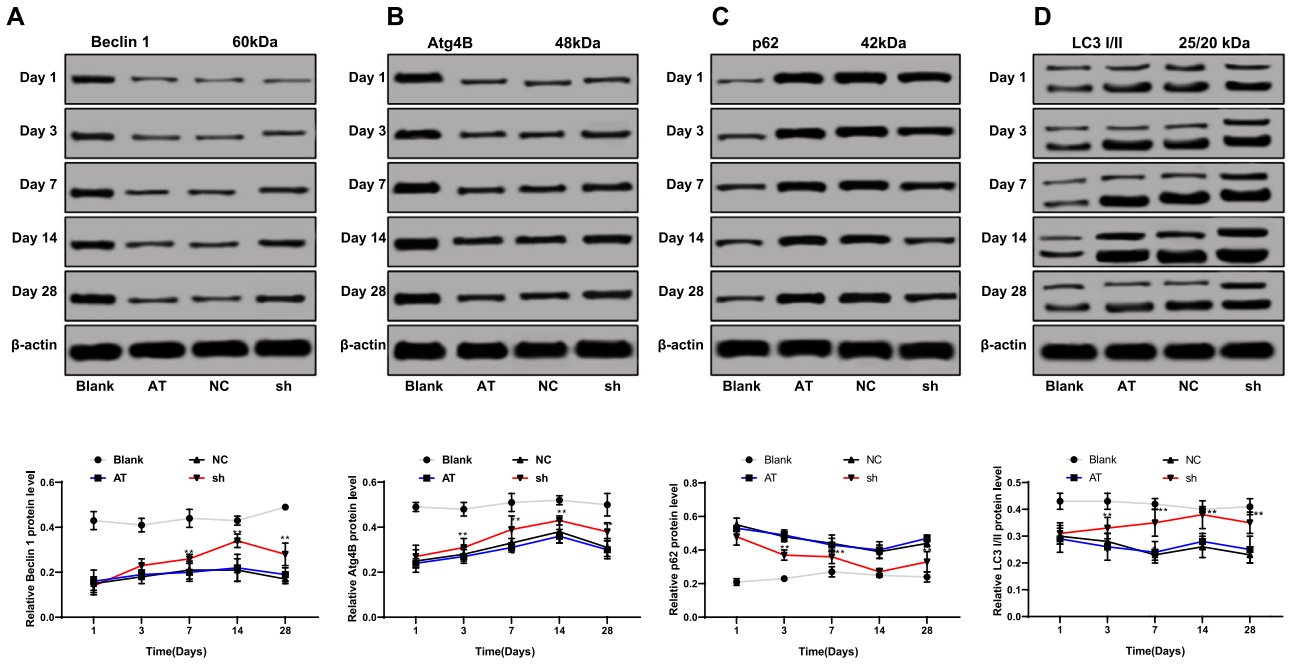

Figure 2. Silencing of S100A4 contributed to promotion of autophagy after corneal alkali burn in rabbits. The protein levels of LC3, Beclin 1 (**A**), Atg4B (**B**), p62 (**C**), and LC3 (**D**) in the cornea after S100A4 silencing were detected by Western blot assay. On days 1, 3, 7, 14, and 28, corneas of three New Zealand white rabbits from each group were used for Western blot assay. Data are expressed as mean ± standard deviation. Replicates = 3. Two-way ANOVA and Tukey's multiple comparisons test were used for data analysis. $^{*}P < 0.05$. $^{**}P < 0.01$.

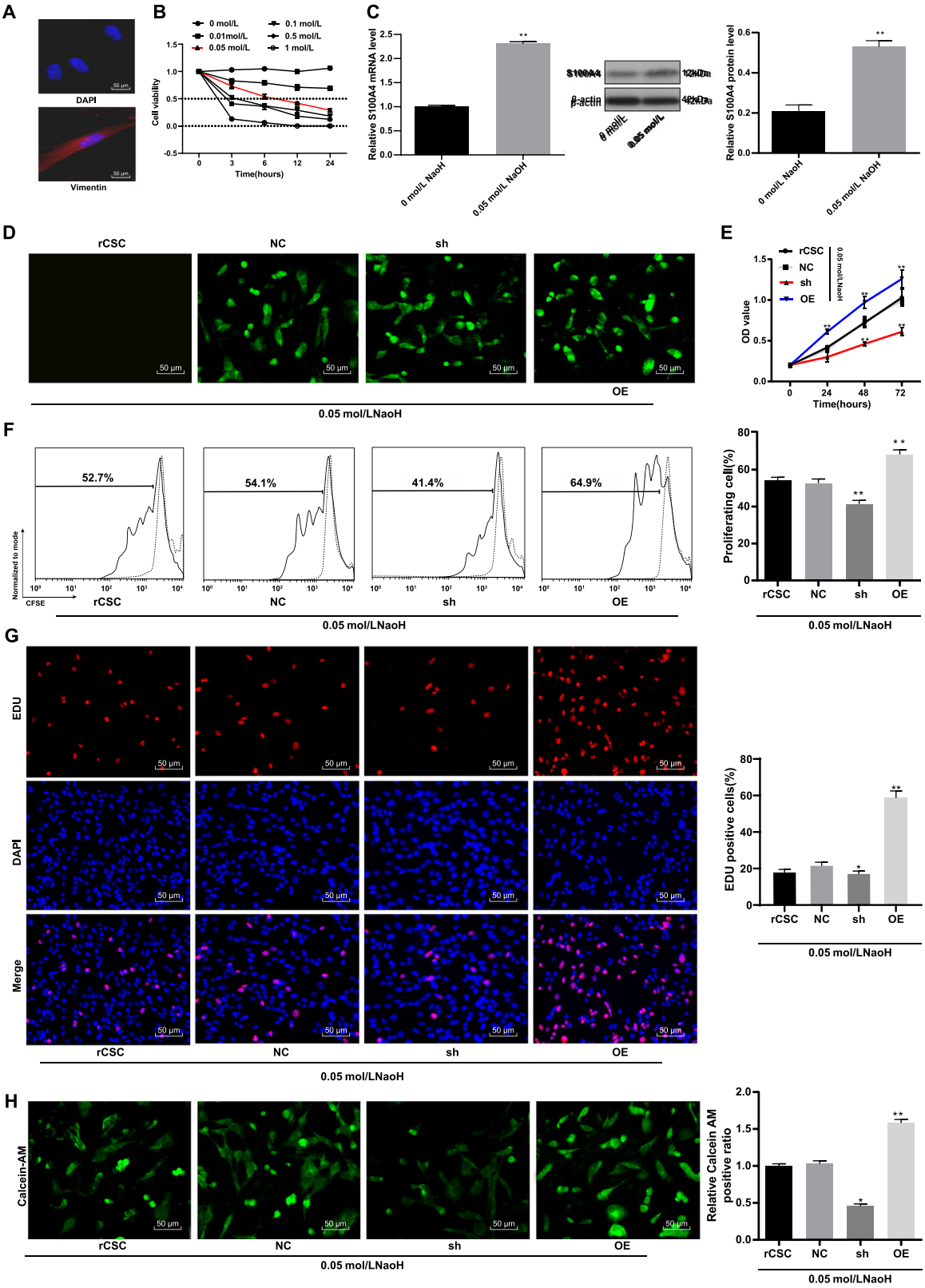

Figure 3. Silencing of S100A4 resulted in reduced viability of rCSCs in a corneal alkali burn model. Detection of rCSCs-specific marker vimentin by immunocytochemistry (**A**); construction of alkali burn rCSC model using different concentrations of NaOH and detection of rCSC viability by MTT assay (**B**); mRNA and protein levels of *S100A4* (S100A4) in NaOH-treated and normal rCSCs by RT-qPCR and Western blot assay (**C**); detection of *S100A4* transfection efficiency by a fluorescence microscope (**D**); detection of cell viability using MTT assay (**E**); rCSCs were stained with CFSE and planted into six-well plates. The cells were collected and detected by flow cytometry after 48 hours (**F**); detection of cell proliferation by EdU labeling assay (**G**); calcein-AM staining for viable cells (**H**). Replicates = 3. Data are expressed as mean ± standard deviation. Two-way or one-way ANOVA and Tukey's multiple comparisons test were used for data analysis. $^{*}P < 0.05$. $^{**}P < 0.01$.

Investigative Ophthalmology & Visual Science

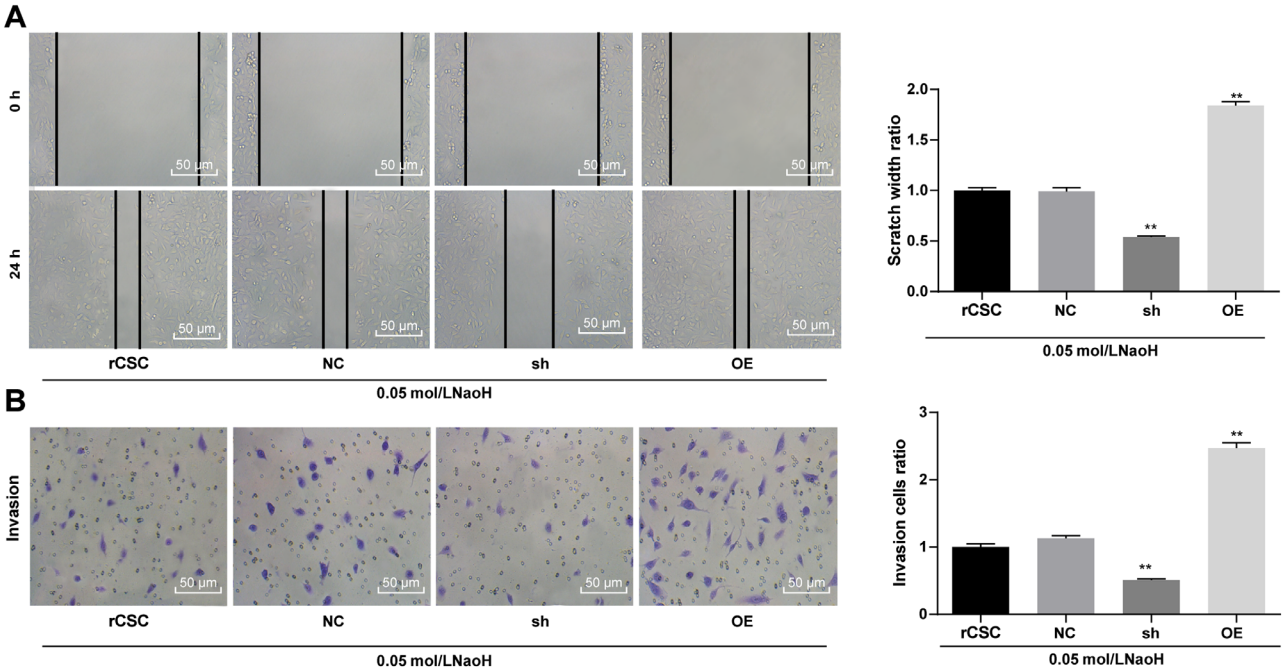

Figure 4. Silencing of S100A4 suppressed the migration and invasion abilities of rCSCs following corneal alkali burn. *S100A4* shRNA vector, overexpressed *S100A4* vector, and NC vector were constructed and transfected into rCSCs after alkali burn modeling. The migration and invasion abilities of rCSCs after alkali burn were measured by scratch test (**A**) and Transwell assay (**B**). Replicates = 3. Data are expressed as mean ± standard deviation. Two-way or one-way ANOVA and Tukey's multiple comparisons test were used for data analysis. $^{*}P < 0.05$. $^{**}P < 0.01$.

of tears, we used the Schirmer test to monitor the amount of tears. The results exhibited that the amount of tears was elevated in the sh group compared with that in the NC group ($P < 0.05$) (Fig. 1C). After corneal damage, corneal stromal cell fibrosis is the main cause of visual impairment,[17] so the level of α-smooth muscle actin (α-SMA) in the cornea was measured by Western blot assay. The results showed that the protein level of α-SMA in the cornea of rabbits with alkali burn was significantly reduced after S100A4 silencing (all $P < 0.05$) (Fig. 1D). RT-qPCR and Western blot assays displayed that the mRNA and protein levels of *TNF*-α were diminished after *S100A4* silencing at each time point (all $P < 0.05$) (Fig. 1E), consistent with the TNF-α levels in aqueous humor measured by the ELISA assay (all $P < 0.05$) (Fig. 1G). Then, hematoxylin and eosin staining was carried out on the cornea to observe the inflammatory cells in the cornea at each time point. The number of inflammatory cells in the cornea of rabbits with alkali burn increased on day 1 and reached the maximum value on day 7, and the number of inflammatory cells began to decrease on day 14 and tended to be stable on day 28. The pathologic degree of cornea in the sh group was significantly improved compared with that in the AT group (Fig. 1H). Those data together suggested that silencing S100A4 improved corneal wound healing after alkali burn.

S100A4 Silencing Facilitates Autophagy Following Corneal Alkali Burn

It was reported that S100A4 promotes the occurrence, metastasis, and invasion of various tumors by inhibiting autophagy of tumor cells.[18,19] Therefore, the expressions of autophagy-related proteins (LC3, Beclin 1, Atg4B, and p62) in the cornea were measured using Western blot assay. LC3, Beclin 1, and Atg4B are the marker molecules of autophagy,[20–22] and their contents are directly proportional to the number of autophagic vesicles. When autophagy occurs, p62 level decreases; when autophagy is inhibited, p62 protein accumulates continuously.[23] The data showed that the protein levels of LC3, Beclin 1, and Atg4B in the rabbit cornea of the sh group increased, while p62 levels decreased (all $P < 0.05$) (Figs. 2A–2D).

S100A4 Silencing Restrains the Viability of rCSCs Following Corneal Alkali Burn

To verify the effect of S100A4 on corneal stromal cells after alkali burn in vitro, we isolated rCSCs and detected the specific marker vimentin by Western blot assay. The results confirmed that the cultured cells were rCSCs (Fig. 3A). After experiments with different concentrations of NaOH on the viability of rCSCs at different time points, 0.05 mol/L and 6 hours were selected as the most suitable sodium hydroxide concentration and time to construct the alkali burn rCSC model (Fig. 3B). Afterward, we compared the mRNA and protein levels of *S100A4* (S100A4) between the NaOH-treated cells and the normal cells. The results showed that S100A4 levels were higher in NaOH-treated rCSCs than in normal rCSCs (Fig. 3C).

To further investigate the effect of S100A4 on corneas after alkali burn, we constructed a green fluorescent protein

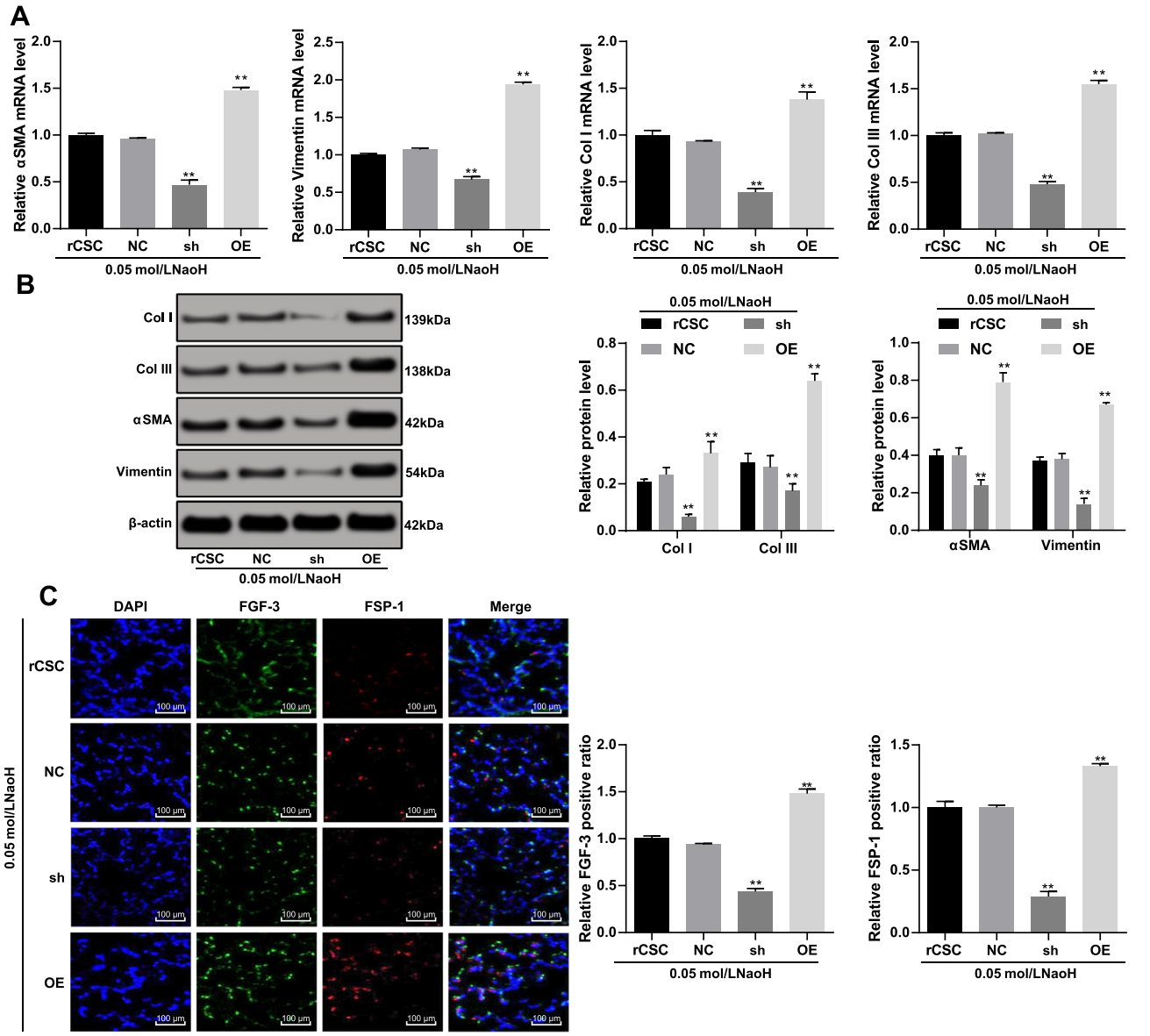

Figure 5. Silencing of S100A4 suppressed the fibrosis of rCSCs induced by corneal alkali burn. *S100A4* shRNA vector, overexpressed *S100A4* vector, and NC vector were constructed and transfected into rCSCs after alkali burn modeling. RT-qPCR and Western blot assay showing mRNA (**A**) and protein (**B**) levels of α-*SMA* (α-SMA), *vimentin* (vimentin), and type I/III collagen in rCSCs after alkali burn; immunofluorescence assay showing FGF-3-positive and FSP-1-positive cells in rCSCs after alkali burn (**C**). Replicates = 3. Data are expressed as mean ± standard deviation. Two-way or one-way ANOVA and Tukey's multiple comparisons test were used for data analysis. $^{*}P < 0.05$. $^{**}P < 0.01$.

(GFP)–carried *S100A4* overexpression vector, sh-*S100A4* vector, and empty vector to be transfected into rCSCs of alkali burn models. After 48 hours of transfection, green fluorescence under the fluorescence microscope suggested successful transfection (Fig. 3D). The cell viability detected by the MTT assay was reduced in the sh group but enhanced in the OE group (Fig. 3E). Flow cytometry exhibited that the proliferation of rCSCs transfected with sh-*S100A4* had a significant decrease, while the proliferation of rCSCs transfected with overexpressed *S100A4* increased (Fig. 3F). The results from EdU labeling and calcein-AM staining showed that the proportion of EdU-positive cells and the number of viable cells decreased in the sh group but were elevated in the OE group (Figs. 3G, 3H). Together, silencing *S100A4* inhibited the viability of rCSCs following corneal alkali burn.

S100A4 Silencing Restrains the Migration and Invasion of rCSCs Following Corneal Alkali Burn

We performed a scratch test to detect the cell migration ability of each group. The results showed that the cell migration rate of the sh group was significantly lower than that of

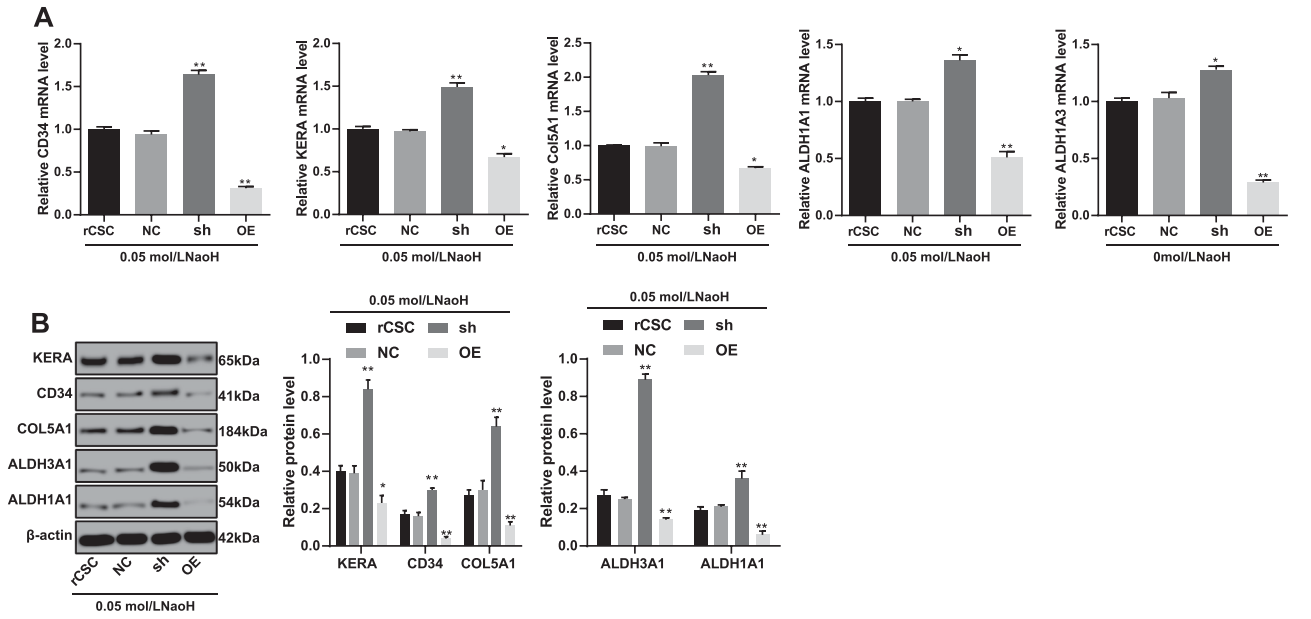

Figure 6. Silencing of S100A4 induced differentiation of rCSCs following corneal alkali burn. *S100A4* shRNA vector, overexpressed *S100A4* vector, and NC vector were constructed and transfected into rCSCs after alkali burn modeling. RT-qPCR and Western blot assay showing mRNA (**A**) and protein (**B**) levels of *CD34* (CD34), *keratocan* (KERA), *COL5A1* (COL5A1), *ALDH1A1* (ALDH1A1), and *ALDH1A1* (ALDH3A1) in rCSCs in the corneal alkali burn model. Replicates = 3. Data are expressed as mean ± standard deviation. Two-way or one-way ANOVA and Tukey's multiple comparisons test were used for data analysis. $^{*}P < 0.05$. $^{**}P < 0.01$.

NC group, while that of OE group was significantly higher (Fig. 4A). The results of the Transwell assay showed the same trend (Fig. 4B).

S100A4 Silencing Inhibits Fibrosis of rCSCs Following Corneal Alkali Burn

Corneal stromal cell fibrosis is the main cause of visual impairment.[16] The mRNA and protein levels of α-*SMA* (α-SMA), *vimentin* (vimentin), and type I/III collagen were reduced in the sh group, which were opposite to the OE group (Figs. 5A, 5B). The fibroblast growth factor (FGF) family plays an important role in cell development, proliferation, migration, and differentiation,[24] and the fibroblast specific protein 1 (FSP-1) is a marker of fibroblasts in tissue-remodeling organs.[25] Therefore, we detected FGF-3-positive and FSP-1-positive expression to assess corneal stromal cell fibrosis. The immunofluorescence assay exhibited that both FGF-3-positive and FSP-1-positive cells were reduced after S100A4 silencing but increased when *S100A4* was overexpressed (Fig. 5C). All those together suggested that inhibition of S100A4 protected rCSCs against cell fibrosis.

S100A4 Silencing Promotes the Differentiation of rCSCs Following Corneal Alkali Burn Into Cornea

To investigate the role of S100A4 in corneal wound healing, we detected levels of cornea-associated protein markers. The results demonstrated that the expressions of CD34 (*CD34*), keratocan (*KERA*), collagen type V alpha 1 chain (*COL5A1*), aldehyde dehydrogenase 1 family member A1 (*ALDH1A1*), and aldehyde dehydrogenase 1 family member A1 (*ALDH3A1*) in rCSCs increased significantly in the sh group but were reduced in the OE group (Figs. 6A, 6B).

S100A4 Silencing Accelerates Autophagy of rCSCs Following Corneal Alkali Burn

The expressions of autophagy-related proteins in rCSCs were detected using RT-qPCR and Western blot assay. The results showed that the mRNA expression of LC3, *Beclin 1* (Beclin 1), and *Atg4B* (Atg4B) in rCSCs increased after *S100A4* silencing while that of *p62* (p62) decreased, accompanied with an increased LC3 II/I (all $P < 0.05$) (Figs. 7A, 7B). Immunofluorescence exhibited that GFP-LC3 cells in the sh group were much more than that in the NC group, and the OE group showed a significant decrease (Fig. 7C). Subsequently, the results of Transmission Electron Microscopy (TEM) showed that the number of autophagosomes was elevated after *S100A4* silencing but reduced when *S100A4* was overexpressed (Fig. 7D). As a consequence, *S100A4* silencing led to promotion of autophagy in rCSCs after alkali burn.

S100A4 Silencing Inhibits the Inflammation and Activation of I3K/Akt/mTOR Signaling Pathway in rCSCs Following Corneal Alkali Burn

The mRNA and protein levels of *VEGF* (VEGF) and *TNF*-α (TNF-α) were reduced when *S100A4* was silenced in rCSCs, and those indexes showed an opposite trend when *S100A4* was overexpressed (Figs. 8A, 8B). Moreover, the PI3K/Akt/mTOR signaling pathway is associated with inflammatory responses and autophagy,[26,27] so we hypoth-

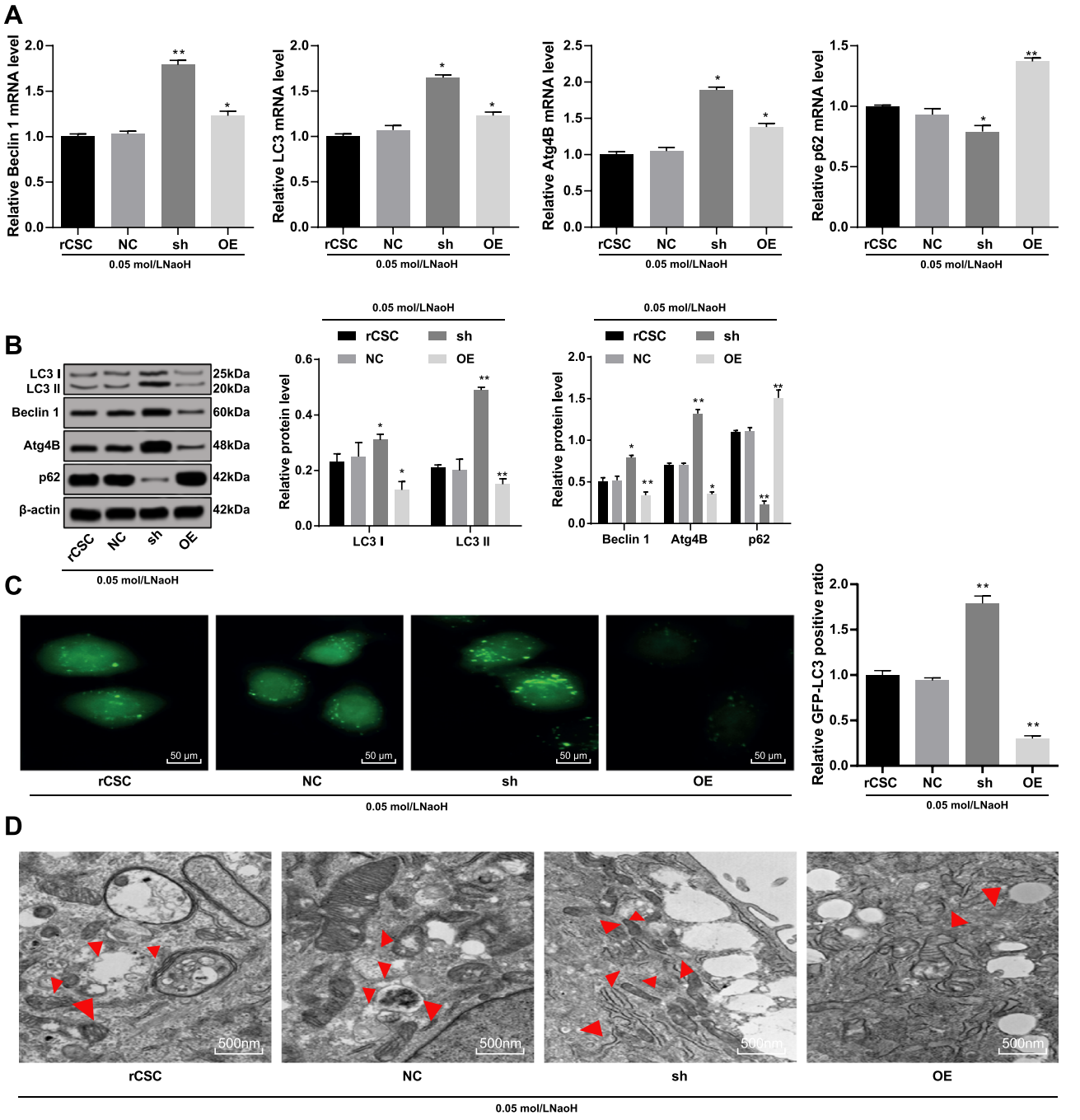

Figure 7. Silencing of S100A4 enhanced the autophagy of rCSCs after alkali burn. *S100A4* shRNA vector, overexpressed *S100A4* vector, and NC vector were constructed and transfected into rCSCs after alkali burn modeling. The mRNA (**A**) and protein (**B**) levels of autophagy-related markers in rCSCs after alkali burn determined by RT-qPCR and Western blot assay; immunofluorescence (**C**) and Transmission Electron Microscopy (TEM) (**D**) showing LC3 protein distribution and the formation of autophagosomes. Replicates = 3. Data are expressed as mean ± standard deviation. Two-way or one-way ANOVA and Tukey's multiple comparisons test were used for data analysis. $^{*}P < 0.05$. $^{**}P < 0.01$. TEM, Transmission Electron Microscopy.

esized that S100A4 might mediate this signaling pathway to regulate inflammation and autophagy. Subsequently, Western blot assay displayed that the phosphorylation of PI3K, Akt, and mTOR in both rabbit cornea and rCSCs was reduced by silencing *S100A4* (Figs. 8C, 8D). Combined with the above results, silencing S100A4 was able to block the PI3K/Akt/mTOR signaling pathway, thereby inhibiting the inflammatory response and autophagy of rCSCs.

S100A4 Inhibits Corneal Wound Healing After Alkali Burn by Activating the PI3K/Akt/mTOR Signaling Pathway

To further validate the effect of S100A4 on the corneal wound healing after alkali burn, we conducted functional rescue experiments. The combined treatment of LY294002 (PI3K-specific inhibitor) and overexpressed *S100A4* was named the IN group, with the OE group as control. The cells

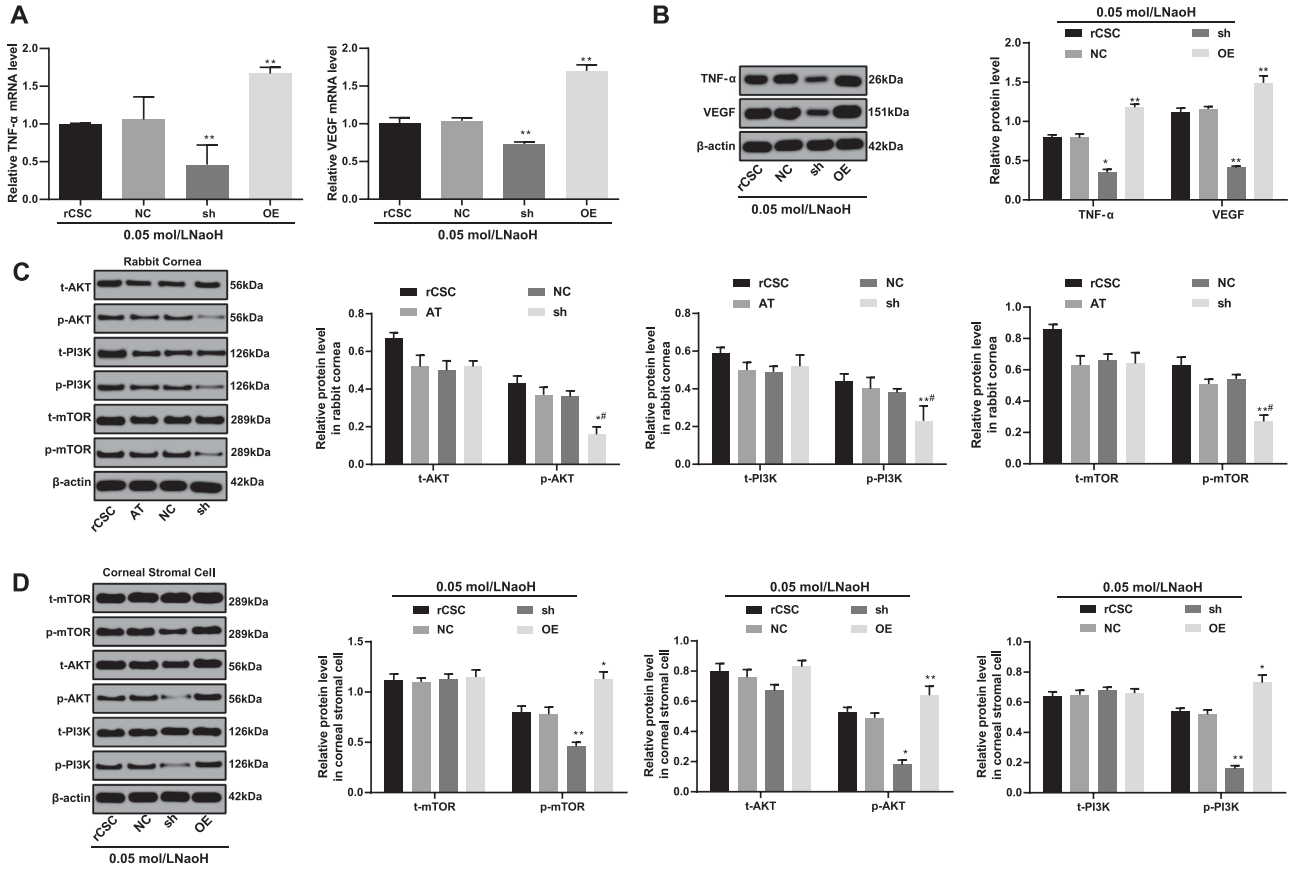

Figure 8. Silencing of S100A4 downregulated the PI3K/Akt/mTOR pathway to inhibit inflammation. The mRNA (**A**) and protein (**B**) levels of *VEGF* (VEGF) and *TNF*-α (TNF-α) in rCSCs after alkali burn determined by RT-qPCR and Western blot assay; the phosphorylation of PI3K, Akt, and mTOR in rabbit cornea (**C**) and rCSCs (**D**) after alkali burn measured by Western blot assay. Replicates = 3. Data are expressed as mean ± standard deviation. Two-way or one-way ANOVA and Tukey's multiple comparisons test were used for data analysis. $^{*}P < 0.05$. $^{**}P < 0.01$.

were collected for subsequent experiments after 24 hours. The phosphorylation of PI3K, Akt, and mTOR; cell viability; cell migration rate; number of invasive cells; and cell fibrosis were reduced notably in the IN group compared with that in the OE group (Figs. 9A–9I). In addition, the differentiation of rCSCs to the cornea and the autophagy were enhanced, while inflammation was inhibited in the IN group (Figs. 9J–9L).

Discussion

Understanding the modulatory roles of S100A4 in fibrosis, neuroprotection, inflammation, and immune response is of potential clinical value for nontumor pathophysiologies.[23,28] This study mainly focused on the roles of S100A4 in wound healing by mediating autophagy and the PI3K/Akt/mTOR signaling pathway. Both the rabbit in vivo model and rCSC in vitro model provide evidence for the promotion effects of S100A4 silencing on corneal wound healing by inhibiting inflammation and facilitating autophagy (Fig. 10).

The first observation of this study was that S100A4 silencing facilitated rabbit corneal wound healing by inhibiting fibrosis and inflammation and promoting autophagy in alkali-burned cornea, as evidenced by increased levels of LC3, Beclin 1, and Atg4B but lowered α-SMA, TNF-α, and p62 levels. Lodder et al.[29] also revealed that autophagy functions as a new anti-inflammatory pathway to regulate liver fibrosis. In a recent study, S100A4 was demonstrated to enhance pulmonary fibrosis via activation of lung fibroblasts.[30] Consistently, inhibition of S100A4 potentially represents a therapeutic strategy against pulmonary fibrosis.[31] Deficiency of S100A4 leads to the alteration of S100A4-lineage cells toward α-SMA^{+} myofibroblasts, driving the promotion of tendon function after acute injury and surgical repair.[32] Ectopic expression of S100A4 has been reported to be implicated in some inflammatory diseases such as airway inflammation in asthma.[33] Knockout of S100A4 in mice dampens the release of proinflammatory cytokines such as TNF-α, IL-6, and IL-17 and thus results in reduction in colon inflammation.[34] Partially coincident with our results, shRNA-mediated suppression of S100A4 enhances the autophagy of lung cancer cells, corresponding to LC3-II protein abundance.[18] In line with our data, the levels of VEGF and TNF-α are reduced by silencing S100A4 in corneal tissues, by which S100A4 affects pathologic CNV induced by alkali burns.[11] In addition, retinal neovascularization can be ameliorated by inhibition of S100A4 in an oxygen-induced retinopathy mouse model.[35,36] On the basis of those findings, our study put forward a way for corneal repair by targeting S100A4.

Next, our study demonstrated that silencing of S100A4 restrained the viability, migration, and invasion of rCSCs in virto.[8,37,38] The promotion in cancer cell migration and

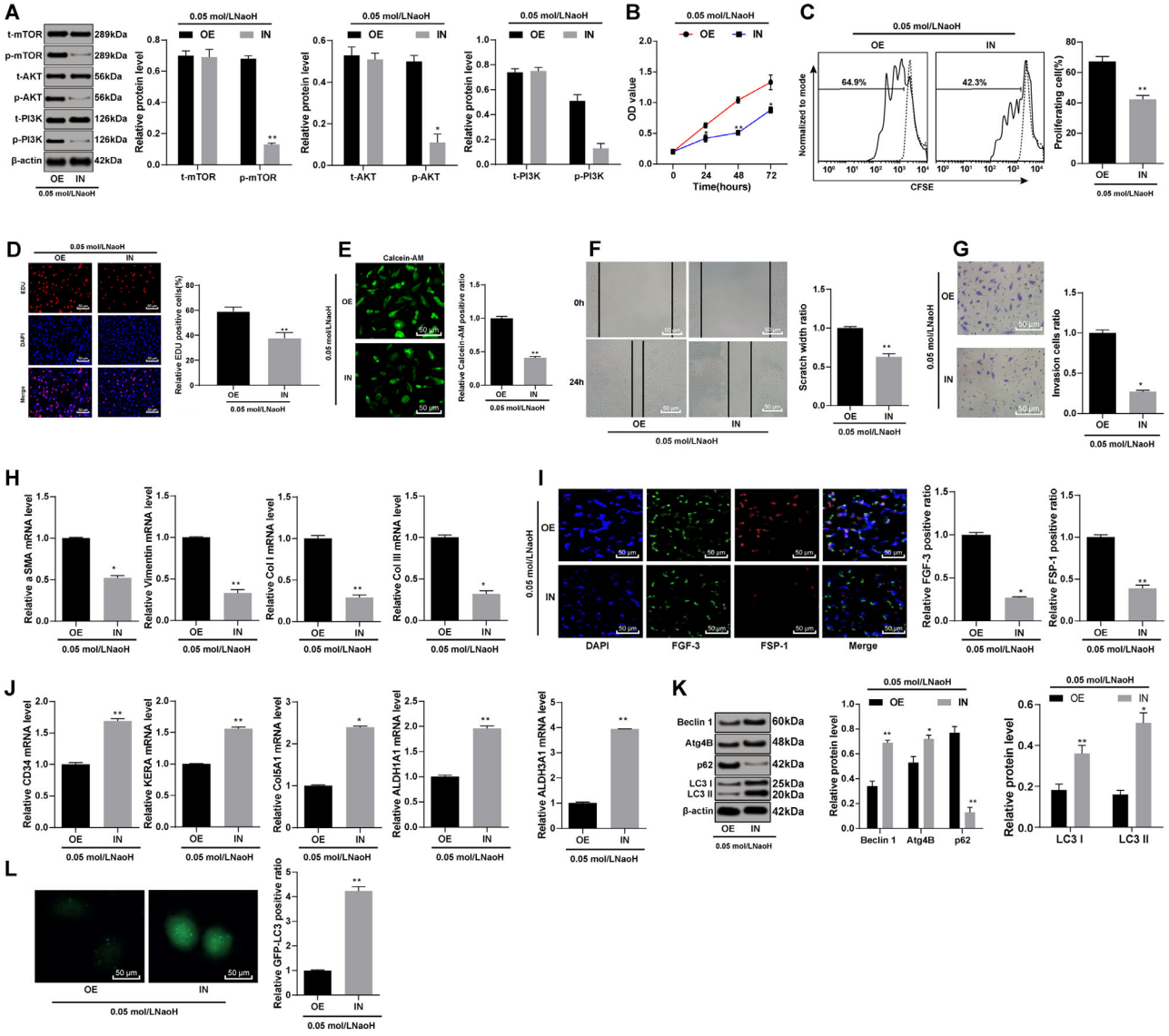

Figure 9. S100A4 inhibited corneal wound healing after alkali burn via activation of the PI3K/Akt/mTOR signaling pathway. *S100A4* shRNA vector, overexpressed *S100A4* vector, and NC vector were constructed and transfected into rCSCs after alkali burn modeling. The phosphorylation of PI3K, Akt, and mTOR measured by Western blot assay (**A**); cell viability detected by MTT assay (**B**); rCSCs were stained with CFSE, planted into six-well plates, and detected by flow cytometry after 48 hours (**C**); cell proliferation detected by EdU labeling assay (**D**); cell viability detected by calcein-AM staining (**E**); migration (**F**) and invasion abilities (**G**) of rCSCs assessed by scratch test and Transwell assay; mRNA levels of *vimentin* and *E-cadherin* detected by RT-qPCR (**H**); FGF-3 and FSP-1 protein expression measured by immunofluorescence (**I**); mRNA levels of corneal cell-specific markers (**J**); levels of autophagy-related markers in rCSCs after alkali burn (**K**); LC3 protein distribution in rCSCs assessed by immunofluorescence. Replicates = 3. Data are expressed as mean ± standard deviation. Two-way or one-way ANOVA and Tukey's multiple comparisons test were used for data analysis. $^{*}P < 0.05$. $^{**}P < 0.01$.

invasion mediated by overexpression of S100A4 has been suggested in several human cancers, such as cutaneous squamous cancer,[39] hepatocellular carcinoma,[40] and squamous cell laryngeal cancer.[41] Our study suggested that S100A4 also modulated those capacities of rCSCs, through which S100A4 silencing was conducive to wound repair. Wound healing is a complex process involving pain and inflammation, proliferation, and excessive scarring (often leading to fibrosis).[42] Then, we found that S100A4 silencing promoted the differentiation of rCSCs following corneal alkali burn into the cornea. During the healing process of corneal stromal cells, the activation of the TGF-β system makes corneal cells transform into myofibroblasts.[43] Myofibroblasts, or activated repair cells, are the main producers and organizers needed to restore tissue integrity after injury.[44] These results above further indicate that S100A4 silencing could improve corneal wound healing after alkali burn.

Subsequently, our study showed that the activation of the PI3K/Akt/mTOR signaling pathway underlay the inhibitory role of S100A4 in corneal wound healing.[45] Meanwhile, S100A4 serves as a renal fibrosis marker reflecting degree of renal fibrosis, which is reduced by dihydroartemisinin with the blockade of the PI3K/Akt pathway.[46] Additionally, the nuclear translocation of S100A4 protein triggered by overexpression of IL-1β in gastric cancer cells is dependent on PI3K activation,[47] and S100A4 promotes migratory

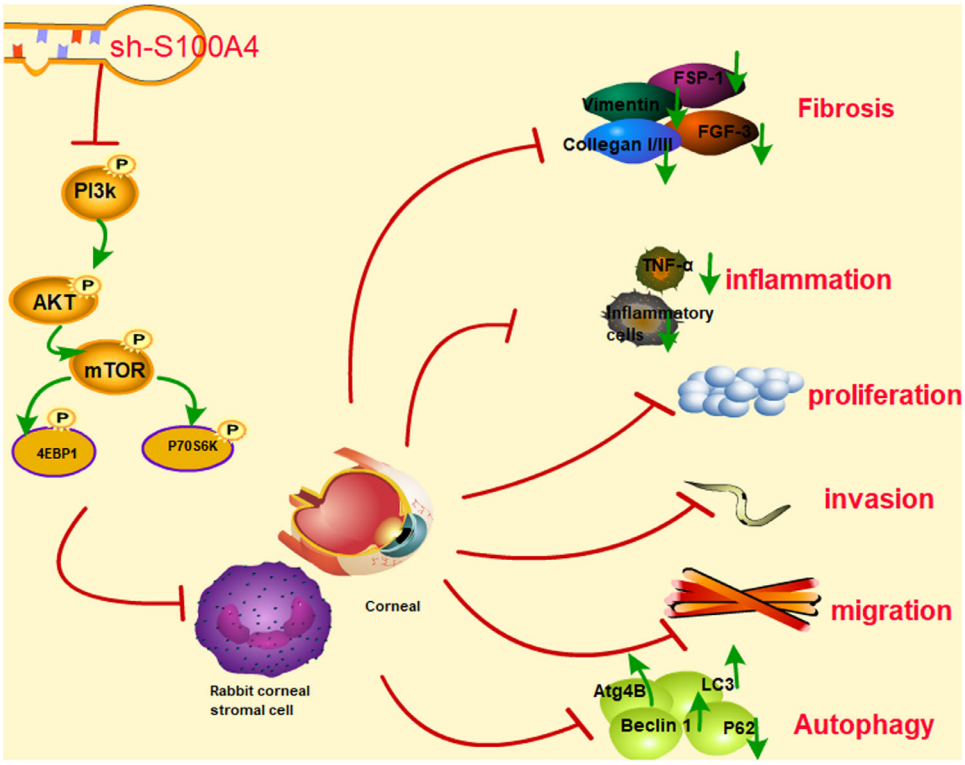

Figure 10. Silencing of S100A4 downregulated the PI3K/Akt/mTOR pathway, enhanced autophagy, and promoted wound healing of rabbit cornea after alkali burn. After S100A4 silencing, the phosphorylation of the PI3K/Akt/mTOR was decreased significantly. The inhibition of the PI3K/Akt/mTOR pathway promoted the autophagy of rCSCs after alkali burn, led to the differentiation of rCSCs into corneal cells, and inhibited the proliferation, invasion, and migration of rCSCs, thereby promoting the wound healing after alkali burn.

and invasive potentials of human esophageal squamous cell carcinoma cells through activation of the Akt signaling pathway.[48] The regulatory network that S100A4 activated the PI3K/Akt/mTOR signaling pathway was confirmed in this study. The PI3K-specific inhibitor reversed the regulatory effects of S100A4 on the biologic functions of rCSCs.

Taken together, silencing S100A4 accelerated corneal healing following alkali burn by inhibiting the PI3K/Akt/mTOR signaling pathway. The understanding of those molecular mechanisms could help to facilitate the development of therapeutic targets for corneal wound healing.[49] We also expected that the role of other signaling pathways in corneal healing could be investigated in future research.

Acknowledgments

Supported by the Science and Technology Plan of Jiangxi Provincial Health and Family Planning Commission (20191037).

Disclosure: **Y. Wang**, None; **G. Gao**, None; **Y. Wu**, None; **Y. Wang**, None; **X. Wu**, None; **Q. Zhou**, None

References

1. Ramponi DR. Chemical burns of the eye. *Adv Emerg Nurs J*. 2017;39:193–198.
2. Ljubimov AV, Saghizadeh M. Progress in corneal wound healing. *Prog Retin Eye Res*. 2015;49:17–45.
3. Bian F, Pelegrino FS, Henriksson JT, et al. Differential effects of dexamethasone and doxycycline on inflammation and MMP production in murine alkali-burned corneas associated with dry eye. *Ocul Surf*. 2016;14:242–254.
4. Ziaei M, Greene C, Green CR. Wound healing in the eye: therapeutic prospects. *Adv Drug Deliv Rev*. 2018;126:162–176.
5. Mohan RR, Tovey JC, Sharma A, Tandon A. Gene therapy in the cornea: 2005–present. *Prog Retin Eye Res*. 2012;31:43–64.
6. Eckert RL, Broome AM, Ruse M, Robinson N, Ryan D, Lee K. S100 proteins in the epidermis. *J Invest Dermatol*. 2004;123:23–33.
7. Li C, Zhang F, Wang Y. S100A proteins in the pathogenesis of experimental corneal neovascularization. *Mol Vis*. 2010;16:2225–2235.
8. Tong L, Lan W, Lim RR, Chaurasia SS. S100A proteins as molecular targets in the ocular surface inflammatory diseases. *Ocul Surf*. 2014;12:23–31.
9. Ryan DG, Taliana L, Sun L, Wei ZG, Masur SK, Lavker RM. Involvement of S100A4 in stromal fibroblasts of the regenerating cornea. *Invest Ophthalmol Vis Sci*. 2003;44:4255–4262.
10. Ambartsumian N, Klingelhofer J, Grigorian M. The multifaceted S100A4 protein in cancer and inflammation. *Methods Mol Biol*. 2019;1929:339–365.
11. Wang YL, Gao GP, Wang YQ, Wu Y, Peng ZY, Zhou Q. Inhibitory effects of S100A4 gene silencing on alkali burn-induced corneal neovascularization: an in vivo study. *Mol Vis*. 2017;23:286–295.
12. Dmytriyeva O, Pankratova S, Owczarek S, et al. The metastasis-promoting S100A4 protein confers neuroprotection in brain injury. *Nat Commun*. 2012;3:1197.
13. Couture C, Desjardins P, Zaniolo K, Germain L, Guerin SL. Enhanced wound healing of tissue-engineered human

corneas through altered phosphorylation of the CREB and AKT signal transduction pathways. *Acta Biomater*. 2018;73:312–325.
14. Cao L, Graue-Hernandez EO, Tran V, et al. Downregulation of PTEN at corneal wound sites accelerates wound healing through increased cell migration. *Invest Ophthalmol Vis Sci*. 2011;52:2272–2278.
15. Wang H, Duan L, Zou Z, et al. Activation of the PI3K/Akt/mTOR/p70S6K pathway is involved in S100A4-induced viability and migration in colorectal cancer cells. *Int J Med Sci*. 2014;11:841–849.
16. Fortunato GM, Da Ros F, Bisconti S, et al. Electrospun structures made of a hydrolyzed keratin-based biomaterial for development of in vitro tissue models. *Front Bioeng Biotechnol*. 2019;7:174.
17. Das SK, Gupta I, Cho YK, et al. Vimentin knockdown decreases corneal opacity. *Invest Ophthalmol Vis Sci*. 2014;55:4030–4040.
18. Hou S, Tian T, Qi D, et al. S100A4 promotes lung tumor development through beta-catenin pathway-mediated autophagy inhibition. *Cell Death Dis*. 2018;9:277.
19. Shen W, Chen D, Liu S, et al. S100A4 interacts with mutant p53 and affects gastric cancer MKN1 cell autophagy and differentiation. *Int J Oncol*. 2015;47:2123–2130.
20. Gozuacik D, Kimchi A. Autophagy as a cell death and tumor suppressor mechanism. *Oncogene*. 2004;23:2891–2906.
21. Rothe K, Lin H, Lin KB, et al. The core autophagy protein ATG4B is a potential biomarker and therapeutic target in CML stem/progenitor cells. *Blood*. 2014;123:3622–3634.
22. Sanches-Silva A, Testai L, Nabavi SF, et al. Therapeutic potential of polyphenols in cardiovascular diseases: regulation of mTOR signaling pathway. *Pharmacol Res*. 2020;152:104626.
23. Mathew R, Karp CM, Beaudoin B, et al. Autophagy suppresses tumorigenesis through elimination of p62. *Cell*. 2009;137:1062–1075.
24. Fei F, Qu J, Li C, Wang X, Li Y, Zhang S. Role of metastasis-induced protein S100A4 in human non-tumor pathophysiologies. *Cell Biosci*. 2017;7:64.
25. Antoine M, Wirz W, Tag CG, et al. Fibroblast growth factor 16 and 18 are expressed in human cardiovascular tissues and induce on endothelial cells migration but not proliferation. *Biochem Biophys Res Commun*. 2006;346:224–233.
26. Tache DE, Firu SG, Andrei AM, et al. Correlation between Tgf-beta1 and Fsp-1 expression in chronic viral hepatitis—an immunohistochemical study. *Curr Health Sci J*. 2015;41:179–185.
27. Wang Z, Zhou L, Zheng X, et al. Autophagy protects against PI3K/Akt/mTOR-mediated apoptosis of spinal cord neurons after mechanical injury. *Neurosci Lett*. 2017;656:158–164.
28. Xue JF, Shi ZM, Zou J, Li XL. Inhibition of PI3K/AKT/mTOR signaling pathway promotes autophagy of articular chondrocytes and attenuates inflammatory response in rats with osteoarthritis. *Biomed Pharmacother*. 2017;89:1252–1261.
29. Lodder J, Denaes T, Chobert MN, et al. Macrophage autophagy protects against liver fibrosis in mice. *Autophagy*. 2015;11:1280–1292.
30. Li Y, Bao J, Bian Y, et al. S100A4(+) macrophages are necessary for pulmonary fibrosis by activating lung fibroblasts. *Front Immunol*. 2018;9:1776.
31. Zhang W, Ohno S, Steer B, et al. S100a4 is secreted by alternatively activated alveolar macrophages and promotes activation of lung fibroblasts in pulmonary fibrosis. *Front Immunol*. 2018;9:1216.
32. Ackerman JE, Nichols AE, Studentsova V, Best KT, Knapp E, Loiselle AE. Cell non-autonomous functions of S100a4 drive fibrotic tendon healing. *Elife*. 2019;8:e45342.
33. Huang X, Qu D, Liang Y, Huang Q, Li M, Hou C. Elevated S100A4 in asthmatics and an allergen-induced mouse asthma model. *J Cell Biochem*. 2019;120:9667–9676.
34. Zhang J, Hou S, Gu J, et al. S100A4 promotes colon inflammation and colitis-associated colon tumorigenesis. *Oncoimmunology*. 2018;7:e1461301.
35. Cheng G, He T, Xing Y. Silencing of S100A4, a metastasis-associated protein, inhibits retinal neovascularization via the downregulation of BDNF in oxygen-induced ischaemic retinopathy. *Eye (Lond)*. 2016;30:877–887.
36. Cheng G, Tian K, Zhang L, Yang N, Xing Y, He T. S100A4 gene silencing in oxygen-induced ischemic retinopathy inhibits retinal neovascularization via down-regulation of CREB expression. *Graefes Arch Clin Exp Ophthalmol*. 2016;254:97–108.
37. Ning Q, Li F, Wang L, et al. S100A4 amplifies TGF-beta-induced epithelial-mesenchymal transition in a pleural mesothelial cell line. *J Investig Med*. 2018;66:334–339.
38. Liu M, Liu J, Yang B, et al. Inversed expression patterns of S100A4 and E-cadherin in cervical cancers: implication in epithelial-mesenchymal transition. *Anat Rec (Hoboken)*. 2017;300:2184–2191.
39. Yu LJ, Li Y, Li C, et al. Restoration of S100A4 expression enhances invasive and metastatic potentials of COLO16 cutaneous squamous cancer cells. *Cancer Biomark*. 2014;14:325–333.
40. Zhang J, Zhang DL, Jiao XL, Dong Q. S100A4 regulates migration and invasion in hepatocellular carcinoma HepG2 cells via NF-kappaB-dependent MMP-9 signal. *Eur Rev Med Pharmacol Sci*. 2013;17:2372–2382.
41. Zhang W, Liu Y, Wang CW. S100A4 promotes squamous cell laryngeal cancer Hep-2 cell invasion via NF-kB/MMP-9 signal. *Eur Rev Med Pharmacol Sci*. 2014;18:1361–1367.
42. Laloze J, Fievet L, Desmouliere A. Adipose-derived mesenchymal stromal cells in regenerative medicine: state of play, current clinical trials, and future prospects [published online June 2, 2020]. *Adv Wound Care (New Rochelle)*.
43. Ljubimov AV, Saghizadeh M. Progress in corneal wound healing. *Prog Retin Eye Res*. 2015;49:17–45.
44. Hinz B. The role of myofibroblasts in wound healing. *Curr Res Transl Med*. 2016;64:171–177.
45. Zuo Z, Zhang P, Lin F, et al. Interplay between Trx-1 and S100P promotes colorectal cancer cell epithelial-mesenchymal transition by up-regulating S100A4 through AKT activation. *J Cell Mol Med*. 2018;22:2430–2441.
46. Zhang B, Liu P, Zhou Y, et al. Dihydroartemisinin attenuates renal fibrosis through regulation of fibroblast proliferation and differentiation. *Life Sci*. 2019;223:29–37.
47. Yu A, Wang Y, Bian Y, et al. IL-1beta promotes the nuclear translocation of S100A4 protein in gastric cancer cells MGC803 and the cell's stem-like properties through PI3K pathway. *J Cell Biochem*. 2018;119:8163–8173.
48. Zhang K, Zhang M, Zhao H, Yan B, Zhang D, Liang J. S100A4 regulates motility and invasiveness of human esophageal squamous cell carcinoma through modulating the AKT/Slug signal pathway. *Dis Esophagus*. 2012;25:731–739.
49. Cerezo LA, Remakova M, Tomcik M, et al. The metastasis-associated protein S100A4 promotes the inflammatory response of mononuclear cells via the TLR4 signalling pathway in rheumatoid arthritis. *Rheumatology (Oxford)*. 2014;53:1520–1526.

Investigative Ophthalmology & Visual Science